Terahertz induced magnetization dynamics in a weak ferromagnet $FeBO_3$

E.A. Mashkovich[1], K. Grishunin[1,2], R.V. Mikhaylovskiy[1], P. Christianen[3], Th. Rasing[1], A.V. Kimel[1,2]

[1]Radboud University, Nijmegen 6525-AJ, the Netherlands, e.mashkovich@science.ru.nl
[2]Moscow Technological University (MIREA), Moscow 119454, Russia,
[3]High field magnetic laboratory, Nijmegen 6525-AJ, the Netherlands

Starting from the seminal work by Beaurepaire et al (1996), ultrafast magnetism became one of the hottest topics in condensed matter research [1]. The interest to this topic has been fueled by the potential to impact information technology and communications. Antiferromagnets have been recently identified as appealing media for ultrafast magnetic recording, THz spintronics and THz magnonics [2-3]. Here we investigate the coupling of nearly single pulse THz pulses to spins in $FeBO_3$ and reveal two distinct mechanisms allowing excitation of spin dynamics in this prototypical antiferromagnet.

Optical pulses from Ti:sapphire amplifier with 4 mJ energy, 110 fs duration and repetition rate of 1 kHz were used to generate terahertz radiation by using tilted front optical rectification technique in $LiNbO_3$ crystal [4]. The generated THz beam was broadened by the pairs of parabolic mirrors and tightly focused onto the $FeBO_3$ crystal. To minimize water absorption and dispersion the terahertz path was purged with nitrogen. We use z-cut $FeBO_3$ crystal mounted in a helium cryostat. To increase Faraday rotation we incline the crystal at 10 degrees [5] with respect to the direction of the external magnetic field, see fig. 1(a). Static optical hysteresis loop for this conditions at temperature 6 K is shown in fig. 1(b).

The waveform of the generated terahertz pulse is shown in fig. 1(c) with the amplitude ~500 kV/cm (magnetic field 160 mT). The corresponding spectrum is shown in inset of the figure and spreads from 0.2 to 2.2 THz.

Another optical beam separated by a beamsplitter is used as an optical probe, which was also focused onto the $FeBO_3$ crystal, see fig. 1(a). Probe polarization rotation due to magneto-optical Faraday effect in the sample was detected using balanced photodetector. By changing time delay between THz and probe pulses, magnon trace was mapped, see fig. 2(a).

In this way we observe excitation of two modes of antiferromagnetic resonance in $FeBO_3$: low frequency quasi-ferromagnetic mode (q-FM) at frequency ~ 20 GHz and high frequency quasi-antiferromagnetic mode (q-AFM) at ~ 480 GHz, see fig. 2(b).

Fig. 2(c) shows scaling of the amplitudes from the fig. 2(b). q-AFM mode depends linearly on the terahertz electric (or magnetic) field (open circles), while q-FM mode scales qudratically (closed circles). The fist dependence is explained by resonant excitation of q-AFM mode by terahertz magnetic field. While generation mechanism of the q-FM mode is off-resonant and similar to the impulsive stimulated Raman scattering by magnons [6].

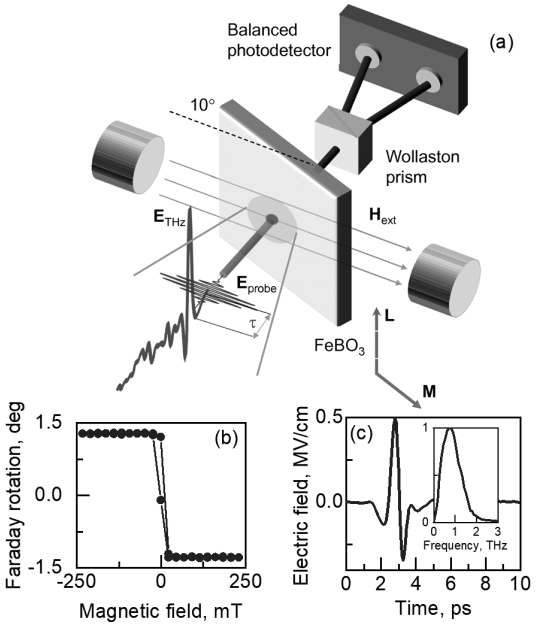

Fig. 1. (a) Experimental scheme. **L, M** are antiferromagnetic and magnetization vectors, respectively. τ is a controllable time delay between THz pump pulse and optical probe pulse. (b) Static hysteresis loop measured with the help of magneto-optical Faraday effect. Temperature is 6 K. (c) Terahertz electric field waveform and the corresponding spectrum (inset).

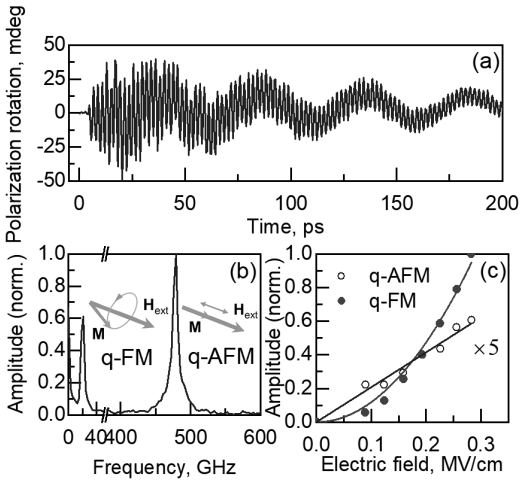

Fig. 2. (a) THz-induced magnetization dynamics at 6 K. (b) Corresponding Fourier spectrum of waveform shown in (a). Insets demonstrate behavior of the magnetization **M**. (c) Scaling of the amplitudes from (b).

Hence we show that intense terahertz pulses efficiently trigger spin dynamics in $FeBO_3$.

References

1. *Beaurepaire, E. et al.*, Ultrafast spin dynamics in ferromagnetic nickel // Phys. Rev. Lett. 1996. V. 76. P. 4250-4253.

2. *Baierl, S. et al.,* Nonlinear spin control by terahertz-driven anisotropy fields // Nat. Photon. 2016. V. 10. P. 715-718.

3. *Baierl, S. et al.*, Terahertz-driven nonlinear spin response of antiferromagnetic nickel oxide // Phys. Rev. Lett. 2016. V. 117. P. 197201.

4. *Hebling, J. et al.*, Velocity matching by pulse front tilting for large-area THz-pulse generation // Opt. Express. 2002. V. 21. P. 1161-1166.

5. *Wolfe, R. et al.*, Room-temperature ferromagnetic materials transparent in the visible // J. Appl. Phys. 1970. V. 41. P. 1218.

6. *Kalashnikova, A.M. et al.,* Impulsive excitation of coherent magnons and phonons by subpicosecond laser pulses in the weak ferromagnet $FeBO_3$ // Phys. Rev. B. 2008. V. 78. P. 104301.

Challenges of Raman scattering at THz frequencies

S. G. Pavlov [1], N. Deßmann [2], N. V. Abrosimov [3], R. Kh. Zhukavin [4], V. N. Shastin [4], and H.-W. Hübers [1,2]

[1]Institute of Optical Sensor Systems, German Aerospace Center (DLR), Berlin, Germany
[2]Department of Physics, Humboldt-Universität zu Berlin, Berlin, Germany
[3]Leibniz Institute of Crystal Growth, Berlin, Germany
[4]Institute for Physics of Microstructures, Nizhny Novgorod, Russia, zhur@ipmras.ru

Wavelength-tunable powerful infrared sources, such as free electron lasers (FELIX Facility at Radboud University, Nijmegen, The Netherlands and CLIO/LCP Facility at Universite Paris Sud, Orsay, France), enable strong nonlinear interaction of light with donor centers in silicon at low lattice temperatures. Despite very low Raman scattering efficiency at such long wavelengths, stimulated Stokes emission has been achieved from silicon crystals doped by different donors at low lattice temperatures when pumped by emission of the infrared FELs (Fig. 1).

Among the factors enabling such phenomena are Raman-active intracenter donor transitions in silicon falling into the THz range and serving as outgoing resonances in electronic Stokes scattering; high-Q laser resonators on total internal reflection modes; large FEL pump photon flux densities (up to a few 10^{25} $cm^{-2}s^{-1}$) and fast repetition rates of the FEL micropulses (between 1 GHz and 25 MHz as lowest). Donor-related Raman stimulated emission occurs in the range 4.2-6.5 THz from natural and isotopically enriched 28-silicon crystals with various dopants from the group-V elements while the free electron laser wavelength was varied between 18 and 41 μm (7.5-16.5 THz) [1].

Study of dynamics of the observed emission shows a transient picosecond-micropulse mode that indicates on significantly larger Raman gain realized in THz Raman silicon lasers.

This research has been partly supported by the EC CALIPSO project for the Transnational access to the European FELs and Synchrotron facilities as well as joint German-Russian program “Research on technological advances of radiation sources of photons and neutrons based on accelerators and neutron sources in cooperation with research organizations and universities of the Federal Republic of Germany” (InTerFEL project, BMBF No. 05K2014 and the RMSE No. RFMEFl61614X0008).

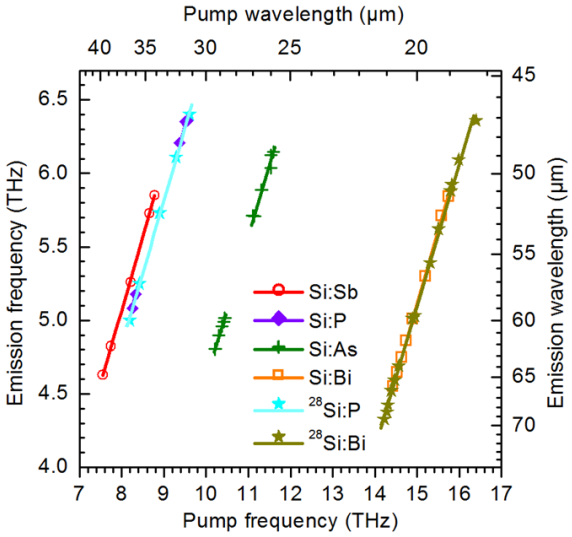

Fig. 1. Stimulated Raman-type THz emission achieved for different dopants in silicon when pumped by pulsed infrared emission from free electron laser (FELIX, micropulse separation is 1 ns). Crystal temperature is about 5K.

Additional support has been from the joint German-Russian project of the German Research Foundation (Deutsche Forschungsgemeinschaft Project No. 389056032) and the Russian Foundation for Basic Research (RFBF Project No. 18-502-12077-DFG). Authors greatly acknowledge technical support provided by the staff of the FELIX and CLIO FEL facilities as well as allocation of the FEL beam time for this study.

References

1. *Pavlov, S. G., Zhukavin, R. Kh., Shastin, V. N., Hübers, H.-W.* The physical principles of terahertz silicon lasers based on intracenter transitions, // Physica Status Solidi (b). 2013. V. 250, P. 9-36.

INTERACTION OF HIGH-POWER TERAHERTZ RADIATION WITH METALLIC FILMS

O. V. Chefonov[1], A. V. Ovchinnikov[1], S. I. Ashitkov[1], S. A. Evlashin[2], P. S. Kondratenko[3], M. B. Agranat[1], V. E. Fortov[1]

[1]Joint Institute for High Temperatures of the Russian Academy of Sciences, Moscow, Russia, oleg.chefonov@gmail.com
[2]Center for Design, Manufacturing and Materials, Skolkovo Institute of Science and Technology, Moscow, Russia
[3]Nuclear Safety Institute of the Russian Academy of Sciences, Moscow, Russia

We report on the experimental observation of high-power terahertz (THz) radiation-induced damage in thin aluminum and nickel films with a thickness less than a terahertz skin-depth. The damage threshold fluence of thin metal films is evaluated for single pulse experiments.

The experiments were performed using a terawatt femtosecond Cr:forsterite laser system, that delivers 100-fs pulses with a bandwidth of 25 nm at a central wavelength of 1240 nm with energy above 80 mJ (energy stability less than 10%) at 10 Hz repetition rate [1]. THz pulses in the range of 1–3 THz were generated by optical rectification of femtosecond laser pulses in organic nonlinear crystal DSTMS (4-N,N-dimethylamino-4-N-methyl-stilbazolium 2,4,6-trimethylbenzene-sulfonate) of 8 mm in diameter [2, 3]. THz low pass filter was used for cutting wavelengths below 34 μm, including the pumping radiation at a wavelength of 1240 nm and its second harmonic at 620 nm generated in nonlinear crystal during optical rectification process. The attenuation coefficient of the THz low pass filter at wavelengths of 1240 nm and 620 nm was more than 10^8. A telescope 6:1 consisted of two off-axis parabolic mirrors with a reflected focus length of 25.4 and 152.4 mm was used to compensate THz beam divergence. The collimated THz beam traveling from the telescope was focused onto a sample using an 90° off-axis parabolic mirror with a reflected focus length of 50.8 mm and a diameter of 50.8 mm to a diffraction-limited spot size. Terahertz pulse energy was measured by means of a calibrated optoacoustic detector (Golay cell) and was up to ~110 μJ at the samples surface.

The samples were a 20-nm Al and Ni films deposited on a glass substrate of 180 μm in thickness using magnetron sputtering of a high-clean metal target (purity of 99.99%) at a rate of 1–1.91 nm/s in an argon atmosphere (purity of 99.999%). The scatter in films thickness were about 1–3 nm from the specified value.

Scanning electron microscope (SEM) images of thin metal film damage patterns at different fluences F of a single THz pulse are presented in Fig. 1 and Fig. 2.

The single-pulse damage threshold of the thin film was experimentally determined using a standard technique, where the squared radius (r_D [μm]) of observed damaged regions is plotted versus the logarithm of the numerical value of the energy of incident THz pulses W_{THz} [μJ] (Fig. 3). This dependence should be linear for a Gaussian beam. Thus, the threshold energy W_{th} could be derived from the line's intersection with an X-axis, while the line's slope determines the parameter of the Gaussian beam at the level of $1/e$.

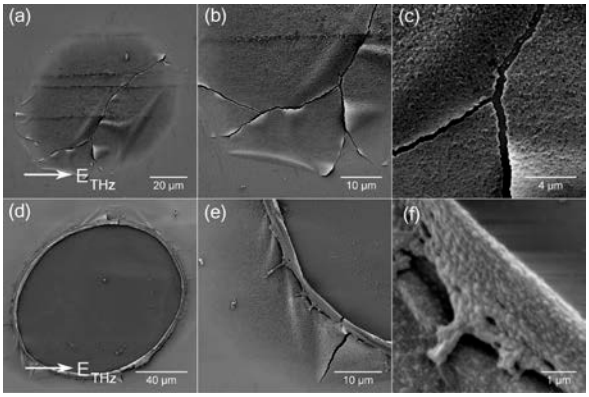

Fig. 1. SEM images of through holes and its edges in Al film produced by single THz pulses. (a), (b), (c): F = 0.14 J/cm^2; (d), (e), (f): F = 0.3 J/cm^2. The arrows indicate the direction of the THz electric field.

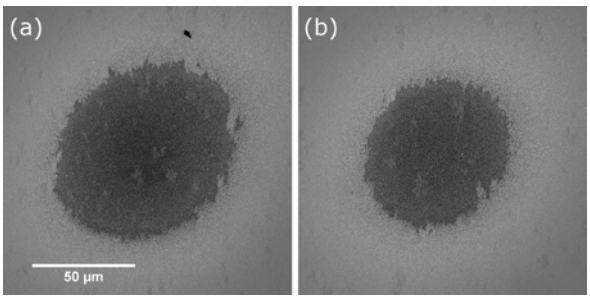

Fig. 2. SEM images of Ni film damages induced by single terahertz pulse at different fluences. (a): F = 0.43 J/cm^2, (b): F = 0.39 J/cm^2. The direction of the THz electric field is the same as in Fig. 1.

The experimental data in Fig. 3 are well approximated with a linear function (solid lines) indicating a Gaussian profile of the terahertz beam, high homogeneity of the used metal film and a distinct threshold behavior of its damage. The measured radius at the level of $1/e$ was of $r_0 \sim 90 \div 92$ μm, which gives a single-pulse damage threshold of the incident fluence of $F_{th} = W_{th}/(\pi\, r_0^2) \approx 0.15$ J/cm^2 for Al and 0.19 J/cm^2 for Ni at an electric-field strength about 15 MV/cm at the center of the focal spot. The value of electric-field strength was estimated using the energy of a THz pulse,

its duration and a focused to a diffraction-limited spot size, assuming a Gaussian pulse shape [2].

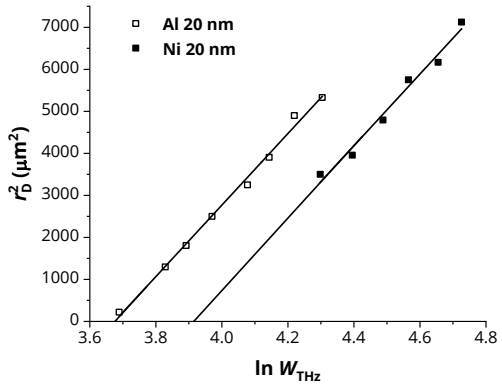

Fig. 4. Determination of the damage threshold in Al and Ni films irradiated with a single THz pulse; experimental data are shown with square symbols approximated with linear functions (solid lines).

SEM images of damage patterns in the Al and Ni films induced by multiple THz pulses at different fluences above the single-pulse damage threshold and number of pulses are shown in Fig. 4 and Fig. 5. The results were obtained at a pulse repetition rate of 10 Hz.

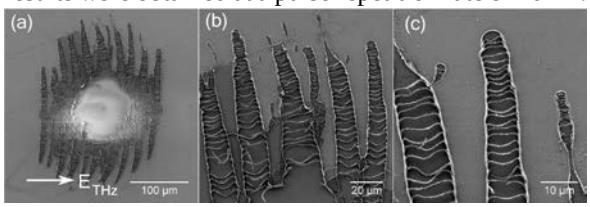

Fig. 4. SEM image of aluminum film damages induced by multiple THz pulses at fluence F = 0.24 J/cm^2, N = 60.

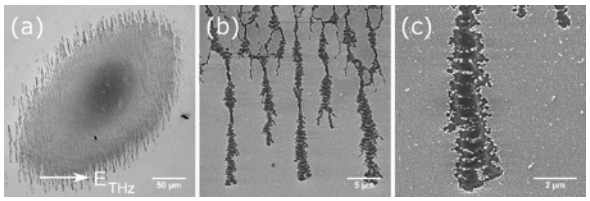

Fig. 5. SEM image of nickel film damage induced by multiple THz pulses at fluence F = 0.43 J/cm^2, N = 40.

We suppose the observed single THz pulse-driven damages in thin metal films to be formed as a result of absorption of the THz pulse energy by conduction electrons with the following generation of hot electrons that transfer energy to the lattice and heat it. Depending on the fluence the lattice heating after the THz pulse could result in film damage due to thermal expansion or melting and ablation processes. Due to differences in acoustical impedances at film boundaries the film center of mass gains momentum in the direction from the substrate. Besides, a tensile stress wave results in adhesive debonding. Delamination of the film occurs when exceeding the adhesion strength. With increasing fluence of the THz pulse the film expands into free space and breaks down.

Damage behavior of metal films irradiated with multiple THz pulses at fluences below the single pulse damage threshold (at the periphery, where according to Gaussian distribution the fluence is below the single-pulse damage threshold) is rather challenging to explain. We suppose that the THz pulse at the center of the focused spot (a region with the peak electric field) generates a microcrack as a result of induced stress. It might be supposed that for the subsequent THz pulses there is a local field enhancement in the gap of the induced microcrack. This results in a microcrack growth perpendicular to the electric-field vector and an increase in width in across-track direction. The microcrack growth occurs along with film ablation in microregions similar to the mechanism of the single pulse damage. As for the Al film, the peripheral damage pattern has the form of elongated surface discontinuities (a kind of channels) that are perpendicular to the electric field vector of the terahertz pulse. However, these “channels” in the Ni film differ in character (pattern) and sizes. For the Al film the observed damages have clearly defined plastic behaviour (the damage surface is smooth, there are smooth and rolled up edges, a rim at the edge of damage is 1–2 μm in width). For the Ni film the damage pattern is similar to fragile or quasi-fragile type (the damaged surface is rough and grainy, there are no smooth edges and rims). This could be associated with different physical and adhesion properties of the films (the Ni film has an increased adhesion as opposed to the Al film), and different processes of the film formation on a substrate during sputtering. Explain the difference in the size and periodicity of the structures formed on the surface of the films is not yet possible. A mechanism related to the generation of such channel-like damages and based on a new phenomenon of electrostriction in thin metal films was proposed in [2], while this phenomenon has not been and could not be observed in bulk metals due to a strong damping of the electric field.

This work is supported by Russian Science Foundation Grant No. 17-19-01261. The experiments were performed using the unique scientific facility ”Terawatt Femtosecond Laser Complex” in the ”Femtosecond Laser Complex” Center of the Joint Institute for High Temperatures of the Russian Academy of Sciences.

References

1. *Agranat, M. B., Ashitkov, S. I., Ivanov, A. A., Konyashchenko, A. V., Ovchinnikov, A. V., Fortov, V. E.* Terawatt femtosecond Cr:forsterite laser system // Quantum Electron. 2004. V. 34, No. 6. P. 506–508.

2. *Agranat, M. B., Chefonov, O. V., Ovchinnikov, A. V., Ashitkov, S. I., Fortov, V. E., Kondratenko, P. S.* Damage in a Thin Metal Film by High-Power Terahertz Radiation // Phys. Rev. Lett. 2018. V. 120, P. 085704.

3. *Chefonov, O. V., Ovchinnikov, A. V., Evlashin, S. A., Agranat, M. B.* Damage Threshold of Ni Thin Film by Terahertz Pulses // has been accepted for publication in Journal of Infrared, Millimeter, and Terahertz Waves.

Disappearance of Self-Focusing for Few-Cycle THz Pulses

S. A. Kozlov[1], A. A. Drozdov[1], M. A. Kniazev[1], D. A. Kislin[1], S. Choudhary[2,3], R. W. Boyd[2,3]

[1] ITMO University, Saint-Petersburg, Russia, kozlov@mail.ifmo.ru
[2] University of Ottawa, Ottawa, Canada
[3] The Institute of Optics, University of Rochester, Rochester, NY 14627-0186, USA

In the present work, we demonstrate that, for few-cycle wave packets with longitudinal dimension less the transverse size, the concept of critical power of self-focusing can lose its physical meaning because of the dominance of dispersion over diffraction. We present simple formulas for the estimation of the parameters of the field and medium under which self-focusing disappears and illustrate with numerical calculations the changes in the self-action phenomenon of light in this case.

Theoretical estimations

We have shown that when the nonlinearity of the optical medium competes primarily not with diffraction but with dispersion, the concept of critical power for self-focusing of radiation P_{cr} will begin to lose its original meaning. Such condition can be expressed in terms of laboratory parameters as:

$$\frac{l_0}{D_0} < \sqrt{c\omega_0 n(\omega_0)\beta_2}\,, \qquad (1)$$

where $l_0 = 2c\tau_0$ is longitudinal size of the wave packet and $D_0 = 2r_0$ is its transverse size, c is the speed of light in vacuum, τ_0 and r_0 are the duration and radius of the beam at the entrance of nonlinear medium, ω_0 is the central frequency of radiation, $n(\omega_0)$ is the linear refractive index of the medium at central frequency, and $\beta_2 = \left(\partial^2 k/\partial\omega^2\right)_{\omega_0}$, where k is the wave number.

For an extremely simple dispersion formula of $n(\omega) = N_0 + ac\omega_0^2$, where N_0 and a characterize the medium dispersion, the inequality (1) can be reduced to

$$\frac{l_0}{D_0} < \sqrt{6N_0\Delta n_{disp}}\,, \qquad (2)$$

where $\Delta n_{disp} = ac\omega_0^2$ is the change of the refractive index at the central wavelength due to dispersion.

Numerical illustrations

We consider boundary conditions (the electric field of radiation at the entrance to nonlinear medium) in the form of a Gaussian axisymmetric paraxial beam with a small number of oscillations ($N = \tau_0 / T_0$)

$$E(0,r,t) = E_0 \exp\left(-\frac{r^2}{r_0^2}\right)\exp\left(-\frac{t^2}{\tau_0^2}\right)\sin(\omega_0 t), \quad (3)$$

where $r = \sqrt{x^2 + y^2}$, and $T_0 = 2\pi/\omega_0$ is central period of electric field oscillations.

The pulse propagation was modeled in terms of the evolution of the instantaneous electric field [1, 2] and not its envelope. The use of the field equation allows on the correctly describe the generation of radiation at tripled and higher frequencies [1]. We show two-dimensional plots of the electric field distribution in Figures 1-3. The light-grey and dark-grey areas correspond to maximum positive and negative values of the electric field, while white lines correspond to zero field values, respectively.

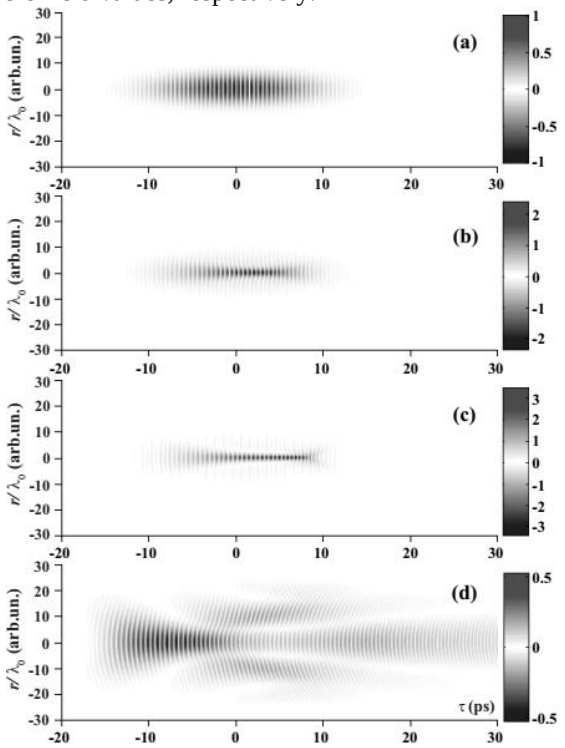

Fig. 1. The spatiotemporal dynamics of the electric THz field E of wave packet (3) in a $MgO:LiNbO_3$ crystal at distances (a) z = 0 cm, (b) z = 8 cm, (c) z = 11 cm, (d) z = 25 cm. Initial pulse parameters are λ_0 = 300 μm, $r_0 = 5\lambda_0$, τ_0 = 8 ps, $I = 3 \times 10^8$ W/cm^2, $P_0 = 4P_{cr}$. We see that the beam shows self-focusing behavior at 8 and 11 cm and the beginning of breakup into filaments at 25 cm

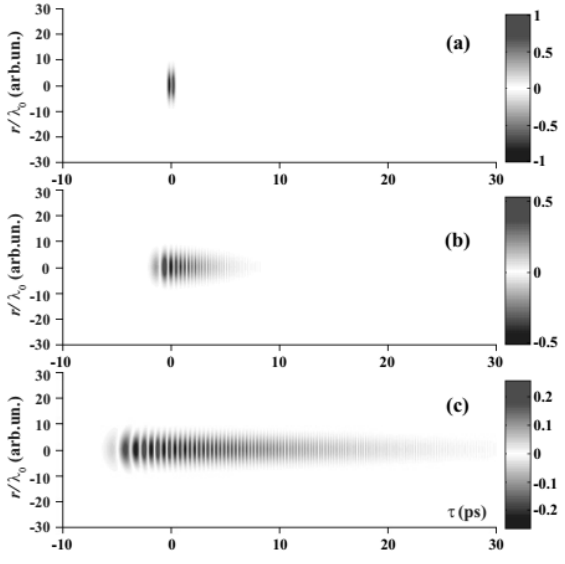

Fig. 2. The spatiotemporal dynamics of the electric field for a single-cycle THz wave packet (3) in a MgO:$LiNbO_3$ crystal at distances (a) z = 0 cm, (b) z = 0.5 cm, (c) z = 2 cm. Initial pulse parameters are λ_0 = 300 μm, $r_0 = 5\lambda_0$, τ_0 = 0.3 ps, $I = 3 \times 10^8$ W/cm^2, $P_0 = 4P_{cr}$. In this case the beam does not display self-focusing

Figures 1 and 2 show typical results for the self-focusing dynamics for a many-cycle pulse (Fig 1) and a single-cycle pulse (Fig 2). The changes in self-focusing dynamics are illustrated for ultrashort pulses with a central wavelength of λ_0 = 300 μm for a number of field oscillations N = 16 ($2\tau_0$ = 16 ps) and N = 0.6 ($2\tau_0$ = 0.6 ps). Stoichiometric MgO:$LiNbO_3$ crystal with nonlinear refractive index $n_2 = 5.4 \times 10^{-12}$ cm^2/W [1] and dispersion parameters described in [1] was considered as the nonlinear dielectric medium. We also used the same ratio between initial power P_0 and critical power P_{cr} for self-focusing, $P_0 = 4P_{cr}$. As can be seen from Fig. 1, at initially stage of THz wave propagation its transverse compression occurs (Fig. 1 b). Then, a shock wave is formed in the generated filament (Fig. 1 c). At the distance of z = 11 cm (Fig. 1 c) a self-focused filament is formed with a transverse size 6.5 times smaller than the input value. The intensity of the radiation increased by a factor of 12 within the filament and reaches a value of 3.6×10^9 W/cm^2. The on-axis pulse duration is seen to decrease by a factor of 1.4 at the e^{-1} level.

With a decreasing of the number of oscillations down to just one (Fig. 2), the dispersion becomes so strong that self-focusing is no longer observed. For example, the axial pulse duration increased in 13 times (at e^{-1} level) already at a distance of z = 5 mm (Fig. 2 b). The curvature of the wave front due to diffraction is noticeable only at the leading edge of the beam. As one can see from Figures 1-2, reduction of N leads to decreasing of self-focusing efficiency because dispersion starts play a significant role in pulse evolution.

For a higher intensity of the input single-cycle THz beam (for example for $I = 1.48 \times 10^{10}$ W/cm^2 such that $P_0 = 200P_{cr}$), we observe an effect that is similar to the phenomenon of self-focusing of radiation (Fig. 1). In contrast to the case considered in Fig. 1, a significant increase of pulse duration is observed here at the initial stage of THz wave propagation because of the combined strong effect of dispersion and nonlinearity. Significant curvature of the wave front due to nonlinearity is also observed (Fig. 3 b,c). At the next step of THz wave propagation, transverse compression occurs due to the curvature. At the distance of z = 44 mm (Fig. 3 d), a filament is formed with transverse dimension 6 times smaller than the input value. However, the intensity of the radiation is decreased down to 5.3×10^9 W/cm^2. In Fig. 3 d we show additionally the result of propagation of the initial beam (Fig. 3 c) in linear dielectric medium 20 mm long with the same dispersion. It can be clearly seen that the focusing occurs in a linear medium as well due to the large curvature of the phase surfaces. Then usual dispersive-diffraction wave packet spreading occurs (Fig. 3 e).

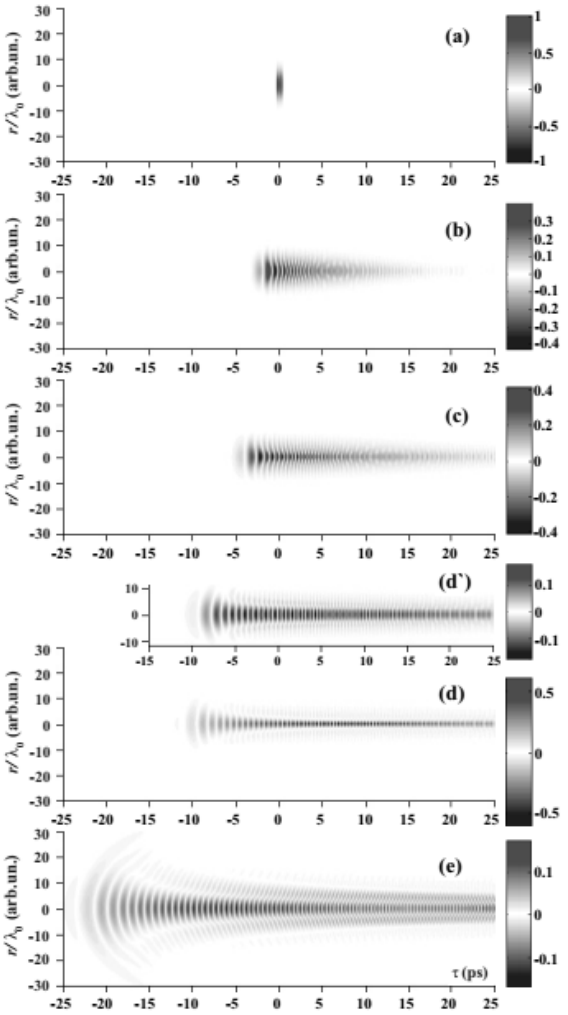

Fig. 3. The spatiotemporal dynamics of the THz electric field E of a single-cycle wave packet (3) in a MgO:$LiNbO_3$ crystal at distances (a) z = 0, (b) z = 9 mm, (c) z = 17 mm, (d) z = 44 mm, (e) z = 90 mm. Initial pulse parameters are λ_0 = 300 μm, $r_0 = 5\lambda_0$, τ_0 = 0.3 ps, $I = 1.48 \times 10^{10}$ W/cm^2, $P_0 = 200P_{cr}$. Case (d‘) corresponds to propagation of the initial beam though a 20-mm-long linear dielectric medium

Conclusion

A simple expression is derived and analyzed for the conditions under which the concept of a critical power for self-focusing loses its fundamental physical meaning due to the dominance of the process of dispersion over diffraction. It is shown that the power of single-cycle terahertz waves, when self-focusing occurs, can exceed the critical power by several hundred times. It is also shown that the nature of the compression of the single-cycle light beam is significantly different from the self-focusing of longer pulses.

References

1. *Drozdov, A. A., Kozlov, S. A., Sukhorukov, A. A., Kivshar, Y. S.* Self-phase modulation and frequency generation with few-cycle optical pulses in nonlinear dispersive media // Phys. Rev. A. 2012. V. 86, No. 5. P. 053822.

2. *Kozlov, S. A., Samartsev, V. V.* Fundamentals of femtosecond optics Woodhead. Cambridge. UK. 2013. P. 272.

Ultrafast multi-electron dynamics studied with THz-field streaking

M. Krikunova[1,2], E. Klimešová[1], O. Kulyk[1], T. Oelze[2], B. Schütte[3], T. Gebert[4], J. Andreasson[1,5]

[1]ELI Beamlines, Dolní Břežany by Prague, Czech Republic, maria.krikunova@eli-beams.eu
[2]Technische Universität Berlin, Berlin, Germany
[3]Max-Born Institute, Berlin, Germany,
[4]Max Planck Institute for the Structure and Dynamics of Matter, Hamburg, Germany,
[5]Chalmers University of Technology, Göteborg, Schweden

Temendous developments of novel ultrafast light sources based on High Harmonic Generation (HHG) or Free-Electron-Lasers (FELs) in the last decade have opened up new experimental regimes in the vacuum-ultraviolet (VUV), extreme-ultraviolet (XUV) down to X-ray spectral regions. Especially, the unique combination of coherent intense radiation with short pulse duration holds very promising perspectives for time-resolved *molecular movies* by obtaining information on molecular structure and function on atomic length scale with time resolution down to the attosecond domain. An understanding of the way how an intense X-ray light interacts with matter is of fundamental importance for studies of molecular structure and dynamics. Therefore this research topic is actively pursued by theoretical and experimental work within the photon science community.

The main objective of the Extreme Light Infrastructure – ELI-Beamlines project – in Dolní Břežany near Prague, Czech Republic is to establish an international user facility for fundamental and applied research with advanced laser sources. The research group for applications in molecular, biomedical, and material sciences works on the development of experimental capabilities using secondary sources that are driven by the unique ELI-Beamlines lasers. A central activity is the development of the multi-purpose user end-station (MAC) for experiments in atomic, molecular, and optical sciences and coherent diffractive imaging. The MAC user end-station is equipped with electron/ion time-of-flight spectrometers, Velocity Map Imaging detector, a detector for coherent diffractive imaging and state-of-the-art sample delivery systems to enable advanced photon science experiments on low density targets (atoms, molecules, clusters, nanometer size single intact free of substrate organic and inorganic particles and crystals, vacuum compatible tens of nanometers to a few micrometers thick liquid sheets formed with gas and by colliding jets technique, cylindrical GDVN jets and aerosols) in a broad range of the electromagnetic spectrum from THz to (soft) X-rays.

The THz-field driven streaking is a novel experimental technique to study the electronic response of many-electron systems to irradiation with intense ultra-short (soft) X-rays pulses [1]. The effect of light-field streaking can be understood as an additional momentum acquired by the free electrons in the presence of a dressing electric field [2]. By changing the time-delay between the ionizing XUV pulse with respect to the streaking field and measuring the electron kinetic energy spectra, a streaking spectrogram is obtained. In the streaking experiment half of the oscillation period of the streaking field has to be shorter than the temporal width of the electron distribution [2]. Therefore, to resolve the electron dynamics that is initiated by the femtosecond (soft) X-ray pulse, a THz-field is used [1].

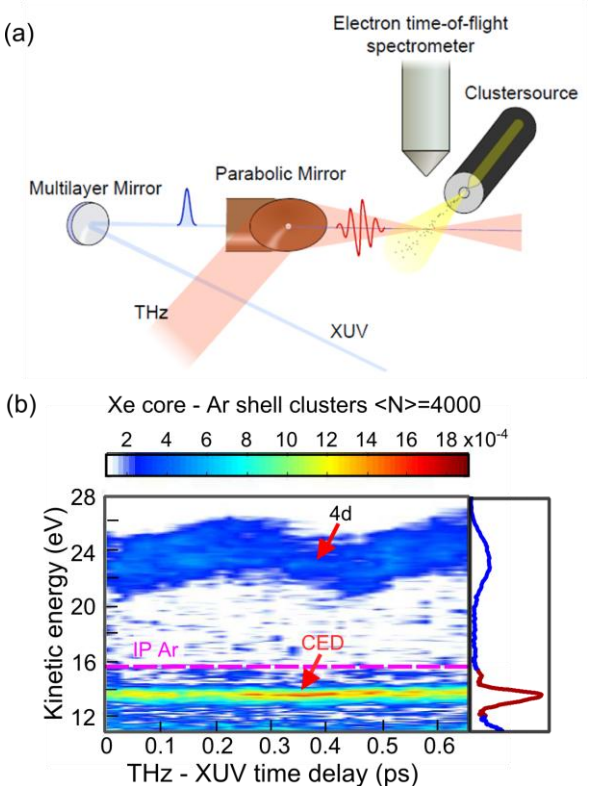

Fig. 1. (a) Principle of the THz-field driven streak-camera measurement. THz and XUV/(soft) X-ray pulses are collinearly overlapped and focused in the interaction region on atomic, molecular or nano-particle target. A series of photoelectron spectra, a so called streaking spectrogram, is measured with an electron-spectrometer as a function of relative time-delay between THz and XUV pulses. **(b)** THz-streaking spectrogram recorded in Xe-Ar clusters at Free-Electron-Laser (FEL) in Hamburg, FLASH. An observation of an un-modulated peak (marked as CED) clearly discloses an electron emission delayed by at least several picoseconds after ionization of Xe-Ar clusters with intense FEL pulses. Data are reproduced from [3].

Figure 1 (a) shows the typical experimental geometry of a THz-streaking experiment [1, 3, 4]. Figure 1 (b) shows an example of a streaking spectrogram recorded upon ionization of Xe-Ar clusters with intense FEL pulses (92 eV photon energy) [3]. In this experiment THz radiation is produced in the THz-undulator by the same electron bunch that is used to produce XUV pulse [1]. Note that electrons released from the 4d orbital of Xe show typical oscillatory behavior due to the shift in electron momentum induced by the instantaneous THz-field at the instance of the electron emission (Figure 1 (b)). Electrons marked as CED (correlated electronic decay), however, remain un-streaked, indicating that these electrons are emitted long after the THz pulse is terminated (i.e. on the time-scale of at least few picoseconds) [3].

For experiments at the MAC user end-station atomic, molecular, cluster or aerosol nano-particles will be available as targets. XUV pulses will be delivered by the HHG-source to the MAC end-station. Two types of THz-sources are planned. The first one is based on the optical rectification in a LiNbO3crystal. To achieve phase matching conditions a tilted-pulse-front geometry will be used [5, 6]. This source typically provides single cycle THz pulses in the frequency range between 0.1 and 1 THz. The expected maximal THz-field strength in the interaction region is ~10 MV/m [4]. The second source of THz radiation is based on difference frequency generation in an organic crystal [7]. This source provides narrow band multi-cycle THz-pulse tunable in the frequency range between 4 and 18 THz. Peak electric field of 370 MV/m has been achieved [7]. Using the same near-infrared laser to drive the HHG process and the THz-source will provide XUV and THz-pulses that are intrinsically synchronized with sub-cycle accuracy [4]. These developments will enable advanced experiments on the structure and dynamics of matter using a combination of THz and HHG beams.

Acknowledgements: This work was supported by the projects Advanced research using high intensity laser produced photons and particles (ADONIS) (CZ.02.1.01/0.0/0.0/16_019/0000789) and Structural dynamics of biomolecular systems (ELIBIO) (CZ.02.1.01/0.0/0.0/15_003/ 0000447) from the European Regional Development Fund and the Ministry of Education, Youth and Sports as part of targeted support from the National Programme of Sustainability II.

References

1. *Frühling, U.., Wieland M., Gensch, M., Gebert, T., Schütte, B., Krikunova,M., Kalms, K., Budzyn, F., Grimm, O., Rossbach, J., Plönjes, E., Drescher, M.*. Single-shot terahertz-field-driven X-ray streak camera // Nature Photon. 2009. V. 3, P. 523–528.

2. *Kienberger, R., Goulielmakis, E., Uiberacker, M., Baltuska, A., Yakovlev, V., Bammerr, F., Scrinzi, A., Westerwalbesloh, T., Kleineberg, U., Heizmann, U., Drescher, M., Krauz, F.*. Atomic transient recorder // Nature, 2004. V. 427. P. 817–821.

3. *Oelze, T., Schütte, B., Müller, M., Müller, J.P., Wieland, M., Frühling, U., Drescher, M., Al-Shemmary, A., Golz, T., Stojanovic, N., Krikunova, M.* Correlated electronic decay in expanding clusters triggered by intense XUV pulses from a Free-Electron-Laser // Sci. Rep. 2017. V. 7, P. 40736.

4. *Schütte, B., Frühling, U., Wieland, M., Azima, A., Drescher, M.*. Electron wave packet sampling with laser-generated extreme ultraviolet and terahertz fields // Opt. Express 2011. V. 19, No. 20. P. 18833–18841.

5. *Hebling, J., Almasi, G., Kozma, I.Z.* Velocity matching by pulse front tilting for large-area THz-pulse generation // Geophys. Opt. Express 2002. V. 10, No. 21. P. 1161–1166.

6. *Yeh, K.L., Hoffmann, M.C., Hebling, J., Nelson, K.A.* Generation of 10 μJ ultrashort terahertz pulses by optical rectification // Appl. Phys. Lett. 2007. V. 90, No. 17. P. 171121.

7. *Liu, B., Bromberger, H., Cartella, A., Gebert, T., Först, M., Cavalleri, A.*. Generation of narrowband, high-intensity, carrier-envelope phase-stable pulses tunable between 4 and 18 THz // Opt. Lett. 2017. V. 42, No. 1. P. 129–131.

Experiments using extreme parameters of the NovoFEL radiation

V. V. Kubarev [1,2], Ya. V. Getmanov[1,2], O. A. Shevchenko[1], E. N. Chesnokov[3], P. V. Koshlyakov[3], L. N. Krasnoperov[4]

[1]Budker Institute of Nuclear Physics, Novosibirsk, Russia, V.V.Kubarev@inp.nsk.su
[2]Novosibirsk State University, Novosibirsk, Russia
[3]Voevodsky Institute of Chemical Kinetics and Combustion, Novosibirsk, Russia
[4]NJIT, New Jersey, USA

Three different types of experimental investigations using unique extreme NovoFEL parameters [1] are presented in the report. The first one is continuous terahertz laser discharge which was developed from an effective demonstration of the NovoFEL power [2] to detailed investigation of its physical process [3-5] and creation of a point-like atmospheric-pressure discharge with record temperature of 28 000 °K at plasma density of $2 \cdot 10^{17}$ cm^{-3} [6](Fig.1-2).

Second set of the experiments is ultrafast time-domain spectroscopy [7-18] used now both for a single-pulse diagnostics of the NovoFEL radiation [11] and in free-induction-decay molecular spectroscopy including a magnetic spectroscopy [15,17](Fig. 3) and spectral "cinema" of the generation/decay dynamics of shot-lived molecular OH-radicals (Fig. 4).

Third type of the experiments is high-resolution spectroscopy based on very good coherency between NovoFEL pulses and very narrow lines of the fine structure of its radiation [19,20] (Fig. 5). One-mode filtration by a set of three resonance Fabry-Perot interferometers allows creation a source of powerful ultramonochromatic tunable radiation for high-resolution molecular spectroscopy [20] (Fig.6).

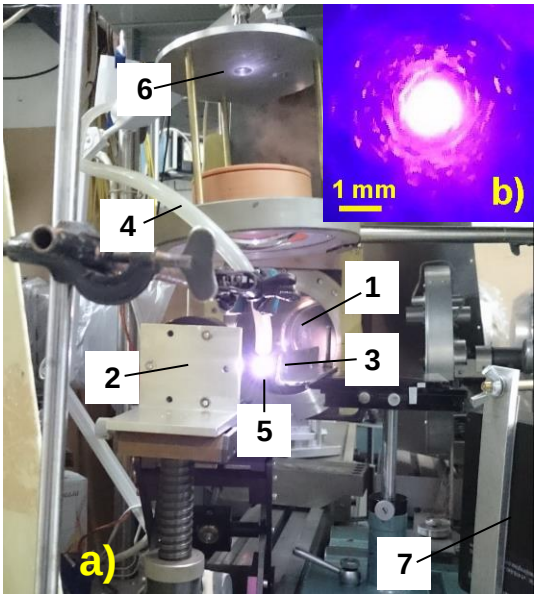

Fig. 1. Experimental setup for investigation of the THz laser discharge (a): 1 – output window of the NovoFEL optical beamline, 2 – main parabolic focusing mirror, 3 – stabilizing spherical mirror, 4 – gas tube, 5 – optical discharge, 6 – ultrafast optical photodiode, 7 – Mightex optical spectrometer. Insert (b) – photo of the point-like high-temperature laser discharge through a navy-blue glass filter

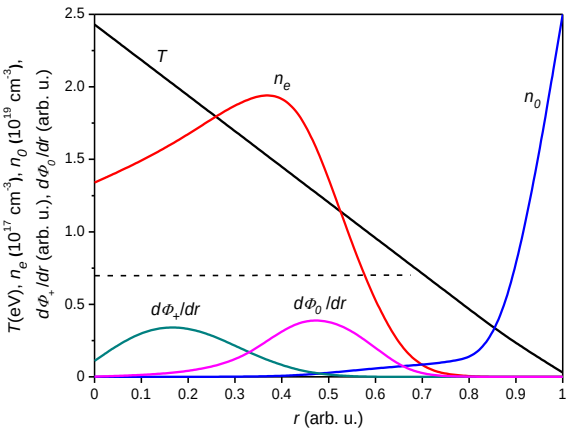

Fig. 2. Radial distributions of temperature T, plasma and gas densities n_e and n_0, and integral radiation of radial spherical layers for ionic $d\Phi_+/dr$ and atomic $d\Phi_0/dr$ lines of argon in the point-like high-temperature laser discharge. The dashed line indicates the critical plasma density (boundary of reflection of THz radiation from plasma)

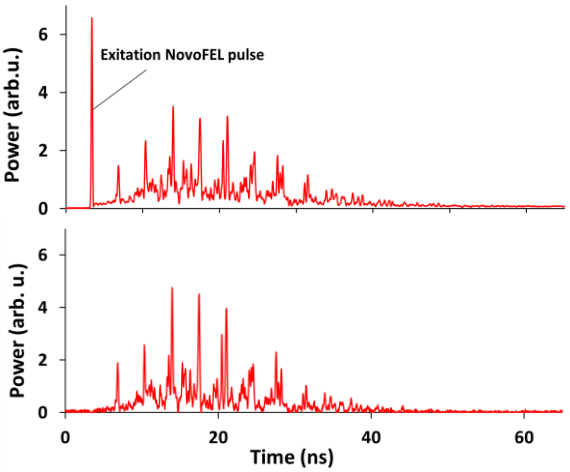

Fig. 3. Polarization separation of powerful excitation NovoFEL pulse and week FID signal of NO_2 molecules in magnetic field: upper – slightly misaligned cross input and output polarizers, lower – exactly aligned cross input and output polarizers (excitation pick is fully dumped)

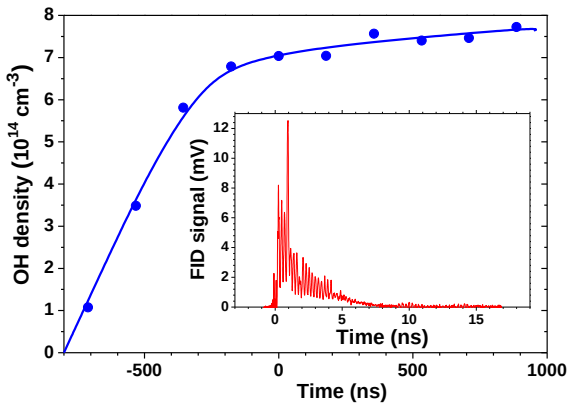

Fig. 4. Dynamics of OH-radical generation after shot pulse of UV radiation: points - treatment of the FID signals (insert) after series of ten NovoFEL excitation diagnostic pulses

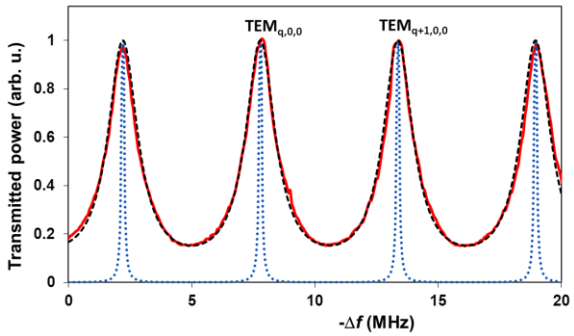

Fig. 5. Fine mode structure of the NovoFEL radiation measured by ultra-long waveguide vacuum mesh resonance FPI: solid red line – experiment, dash black line - instrumental function of the FPI, point blue line – reconstructed longitudinal mode structure of the NovoFEL

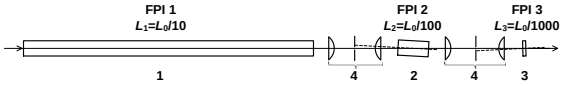

Fig. 6. Optical scheme of setup for one-mode filtration of the NovoFEL radiation: 1-3 – resonance FPI's (1 - ultra-long waveguide vacuum mesh resonance FPI), 4 – optical isolators

This work was made with financial support of Russian Science Foundation (project 14-50-00080). The NovoFEL operation was supported by Ministry of Education and Science of The Russian Federation (project RFMEFI62117X0012).

References

1. *Kulipanov, G. N., et al.* Novosibirsk free electron laser – facility description and recent experiments // IEEE Transaction on Terahertz Science and Technology. 2015. V. 5, No. 5. P. 798-809.

2. *Bolotin, V. P., et al.* Quasi-continuous sub-millimeter optical discharge on Novosibirsk free electron laser: experiments and elementary theory // Proc. IRMMW-THz-2005. 2005. Williamsburg. USA. P. 126–127.

3. *Kubarev, V. V.* Dynamics of the THz optical discharge // Proc. IRMMW-THz-2014. 2014. Tucson. USA. T2-A-16.2.

4. *Kubarev, V. V., Getmanov, Ya. V., Shevchenko, O. A.* Self-oscillations in terahertz laser discharge: Nature, parameters, and suppression // Proc. IRMMW-THz-2016. 2016. Copenhagen. Denmark, DOI:10.1109/IRMMW-THz.2016.7759003.

5. *Kubarev, V. V., Getmanov, Ya. V., Shevchenko, O. A., Koshlyakov, P. V.* Threshold conditions for terahertz laser discharge in atmospheric gases // Journal of Infrared, Millimeter, and Terahertz Waves. 2017. V 38, No. 6. P. 787-798.

6. *Kubarev, V. V., Getmanov, Ya. V., and Shevchenko, O. A.* Continuous point-like high-temperature laser discharge produced by terahertz free //AIP Advances. 2017. V. 7. P. 095123-(1-8).

7. *Kubarev, V., Chesnokov, E., Koshlyakov, P.* Ultrafast high-resolution THz time-domain spectroscopy // Proc. IRMMW-THz-2012. 2012. Wollongong. Australia. Thu-C-2-4.

8. *Kubarev, V., Chesnokov, E., Koshlyakov, P.* Terahertz free induction decay of molecular transitions: direct observation and practical use // Proc. TERA-2012. 2012. Moscow. Russia. P. 68–69.

9. *Chesnokov, E. N., Kubarev, V. V., Koshlyakov, P. V., and Kulipanov, G. N.* Direct observation of the terahertz optical free induction decay of molecular rotation absorption lines in the sub-nanosecond time scale // Appl. Phys. Lett. 2012. V. 101. P. 131109-(1–4).

10. *Kubarev, V. V., Chesnokov, E. N., and Koshlyakov, P. V.* One-pulse high-resolution THz time-domain spectroscopy: development and applications // Proc. IRMMW-THz-2013. 2013. Mainz. Germany. Tu5-5.

11. *Kubarev, V. V.* Ultrafast high-resolution spectroscopy of separate NovoFEL pulses // Proc. IRMMW-THz-2013. 2013. Mainz. Germany. Mo14-4.

12. *Chesnokov, E. N., Kubarev, V. V., Koshlyakov, P. V., Kulipanov, G. N.* Very long terahertz free induction decay in gaseous hydrogen bromide // Laser Phys. Lett. 2013. V. 10. P. 055701-055703.

13. *Chesnokov, E. N., Kubarev, V. V., and Koshlyakov, P. V.* Rotation commensurate echo of asymmetric molecules - Molecular fingerprints in the time domain // Appl. Phys. Lett. 2014. V. 105. P. 261107-(1–4).

14. *Chesnokov, E. N., Kubarev, V. V., Koshlyakov, P. V., Getmanov, Ya. V., Shevchenko, O. A.* Non-Faraday rotation of the free induction decay in gaseous NO // Chemical Physics Letters. 2015. V. 636. P. 203–207.

15. *Chesnokov, E. N., Kubarev, V. V., Koshlyakov, P. V., Chichinin, A. I., Getmanov, Ya. V., Shevchenko, O. A.* The influence of magnetic field on the echo-like free induction decay in NO_2 // Chemical Physics Letters. 2016. V. 662. P. 62–66.

16. *Chesnokov, E. N., Kubarev, V. V., Koshlyakov, P.V.* Observation of the Formation of 0-π Pulses in Rotation Spectra of HCN and HBr // Physics Procedia. 2016. V. 84. P. 135 – 141.

17. *Bragin A.V. et al.* Superconducting solenoid for superfast THz spectroscopy // Physics Procedia. 2016. V. 84. P. 82 – 85.

18. *Chesnokov, E. N., Kubarev, V. V., Koshlyakov, P. V., and Fedorov, V. V.* Heterodyne Method of Detection of Molecular Gas in the Terahertz Region Using the Beats Between Free Induction Decay Signals // IEEE Transactions on terahertz science and technology. 2017. V. 7, No. 2. P. 144–150.

19. *Kubarev, V. V.* Instabilities, coherency, and spectra of the NovoFEL radiation // EPJ Web of Conferences. 2017. V. 149. P. 05007(1-2).

20. *Kubarev, V. V., Getmanov, Ya. V.* NovoFEL as source of powerful ultramonochromatic tunable terahertz radiation // Proc. IRMMW-THz-2018. 2018. Nagoya. Japan. Fr-A2-1b-3.

Vector and mixed beams with orbital angular momentum

N. D. Osintseva[1], Yu. Yu. Choporova[1,2], O. E. Kameshkov[1,2], B. A. Knyazev[1,2], V. S. Pavelyev[3]

[1]Budker Institute of Nuclear Physics SB RAS, Novosibirsk, Russia, natalyaosintseva@gmail.com
[2]Novosibirsk State University, Novosibirsk, Russia
[3]Samara National Research University, Samara, Russia

Introduction

Vector beams with radial polarization are of great interest in surface plasmon science. Surface plasmon generation and propagation require polarization state which is perpendicular to the surface. Hence vector beams increase the generation efficiency of surface plasmon-polaritons on cylindrical metal-dielectric surfaces, such as wires [1].

In this work vector [2] and mixed beams with orbital angular momentum (OAM) [3] were generated by silicon binary diffractive optical elements (DOEs) in the THz range. The radiation was generated by the Novosibirsk free electron laser (NovoFEL), which has the possibility of smooth wavelength tuning from 6 to 220 μm [4]. Hence, we studied the efficiency of DOEs at different wavelengths. Using Fourier filtration diffraction efficiencies of 25-30% can be achieved (except of λ/2 and λ/4).

Vector beams

Three phase plates (Fig.1) transformed a linearly polarized Gaussian beam into Hermit-Gaussian (HG) modes (1,0) and (0,1) and into Bessel beam of first and second order. To reach a phase difference of π at a wavelength of 141 μm we used a profile height of $\Delta h = \lambda / 2(n-1) = 29.1\,\mu m$, where n=3.42 is the silicon refractive index [3]. The electric field of a HG beam (10 or 01) has opposite direction for each of its two maxima and hence, the polarization is opposite as well. Two orthogonally polarized HG beams were combined in an in-line Mach-Zehnder interferometer (Fig. 2). A phase singularity in the center leads to the generation of a vector Laguerre-Gaussian (LG) beam. To achieve an axially polarized beam a vertically (1,0) and a horizontally polarized (0,1) HG beam should be combined. A radially polarized beam is formed by the superposition of orthogonal polarization of both beams (Fig. 3).

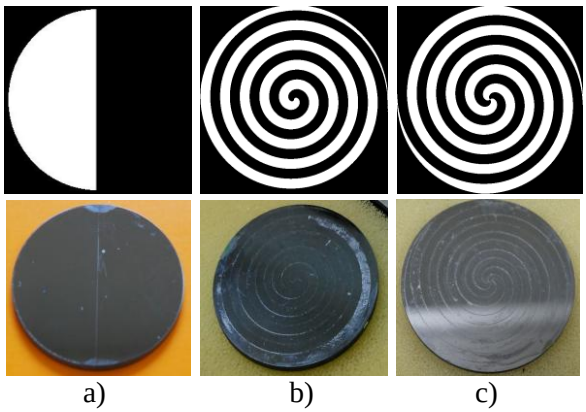

a) b) c)

Fig. 1. Diffractive optical elements for transformation THz Gaussian beam into Hermit-Gaussian (left column) and vortex Bessel beams with topological charges l=1 and l=2 (middle and right columns respectively). The phase distribution (top line) and photo of silicon elements (bottom line). Black zones – phase is 2πN, white zones – πN, where N is integer.

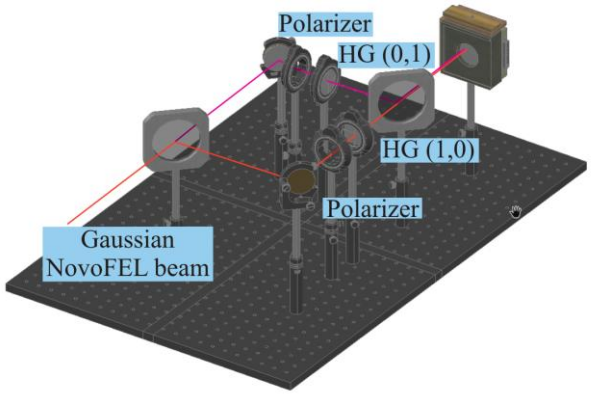

Fig. 2. The experimental scheme of generation a Laguerre-Gaussian vector beam. The Mach-Zehnder interferometer consists of two film beamsplitters and two mirrors. A polarizer and a DOE are situated in each arm f the interferometer.

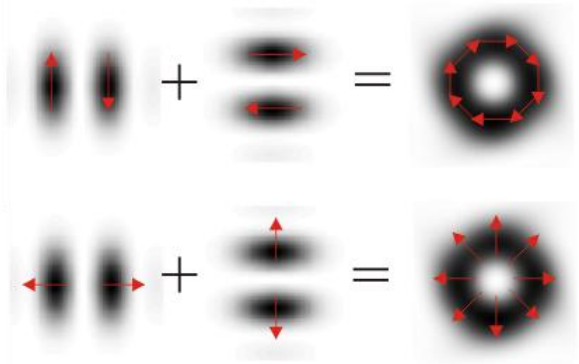

Fig. 3. Principal of generation of a vector beam. Maxima of an intensity distribution is shown with dark color. Red arrows show the direction of polarization. HG (1,0) and HG(0,1) are used to generate Laguerre-Gaussian beam with axial (top line) and radial (bottom line) polarization.

Mixed beams

Mixed beams were generated by combination of Bessel beams with different OAM or vortex beams [6]. A helical wavefront leads to an azimuthal phase dependence in the perpendicular plane. A helical wavefront is characterized by a topological charge, or

helicity. It is equal to the number of times the phase changes from 0 to 2π in the perpendicular plane. Vortex Bessel beams with topological charges ±1 and ±2 were generated by phase binary axicons with spiral zones (Fig. 1) [7]. The sign of the topological charge can be changed by turning the axicon.

Interference patterns of mixed beams with different topological charges are shown in figure 4. The electric field amplitude can be written by the equation:

$$E(r,\varphi,z) = E_0(r,z)e^{i(k_z z + l\varphi)},$$

где $E_0(r,z)$ - complex amplitude, $r = \sqrt{x^2 + y^2}$, φ – azimuthal angle. Thus in a case of superposition of beams with topological charges of -1 and +1 the topological charge is equal to 0.

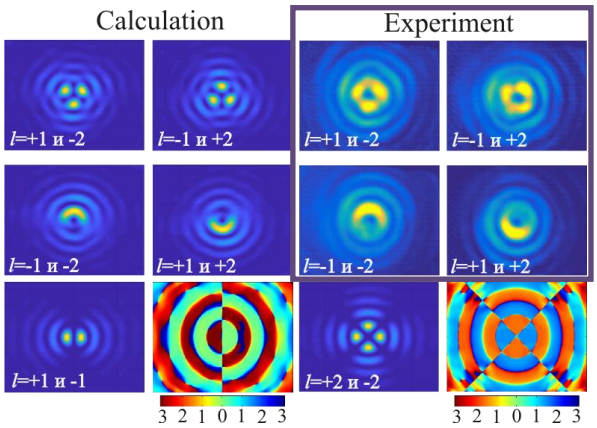

Fig. 4. Calculation and experimental results of mixed beam's generation. Bottom line: calculated intensity and phase distribution for mixed beams with equal values and different signs of topological charges.

Combinations such -1 and +2, or +1 and -2 are more complicated and requier detailed study. If total topological charge is different from the simple ±1 vortex beam we can understand by using vector diffraction theory and plotting a Poynting vector (under development).

References

1. *Weibin, C., Zhan, Q.* Realization of an evanescent Bessel beam via surface plasmon interference excited by a radially polarized beam. // Opt. Lett. 2009. V. 34. P. 722-724.

2. *Oron, Ram, et al.* The formation of laser beams with pure azimuthal or radial polarization. // Applied Physics Letters. 2000. V. 77. No. 21. P. 3322-3324.

3. *Bouchal, Z., et al.* Orbital angular momentum of mixed vortex beams. // 15th Czech-Polish-Slovak Conference on Wave and Quantum Aspects of Contemporary Optics. 2007. Vol. 6609. International Society for Optics and Photonics.

4. *Volodkin, B. O., Choporova, Yu. Yu., Knyazev, B. A., et al.* Fabrication and characterization of diffractive phase plates for forming high-power terahertz vortex beams using free electron laser radiation. // Opt. Quant Electron. 2016. V. 48: No. 4. P. 223.

5. *Agafonov, A. N., et al.* Control of transverse mode spectrum of Novosibirsk free electron laser radiation. // Applied Optics. 2015. V. 54, No. 12. P. 3635-3639.

6. *Allen, L., Beijersbergen, M. W., Spreeuw, R. J. C., Woerdman, J. P.* Orbital angular momentum of light and the transformation of Laguerre–Gaussian laser modes. // Phys. Rev. 1992. V. 45. P. 8185–8189.

7. *Choporova, Yu. Yu., et al.* High-power terahertz non-diffractive bessel beams with angular orbital momentum: Generation and application. // IRMMW-THz 2015: 40th International Conference on Infrared, Millimeter, and Terahertz waves. Hong Kong, 23 - 28 August 2015. - Piscataway: IEEE, 2015. - Art.nr 7327684. - DOI 10.1109/IRMMW-THz.2015.7327684.

Terahertz optical elements for control of high-power laser irradiation

V.S. Pavelyev[1,2], A.N. Agafonov[1,2], B.O. Volodkin[1,2], K.N. Tukmakov[1,2], B.A. Knyazev[3,4], Yu.Yu. Choporova[3,4]

[1]Samara University, Samara, Russia, nano@ssau.ru
[2]Image Processing Systems Institute, Russian Academy of Sciences, Samara, Russia
[3]Budker Institute of Nuclear Physics of SB RAS, Novosibirsk, Russia
[4] Novosibirsk State University, Novosibirsk, Russia

Appearance of the sources of coherent and high power THz radiation [1] opened new horizons for investigations in this frequency range [2]. High attention is focused on silicon diffractive optical elements (DOE), which are used for the beam manipulation [3-7]. The lithographic etching of a silicon substrate has been used in [3-7] to fabricate binary relief of diffractive optical elements. Binary silicon element [4] coated with the antireflection coating remained intact upon exposure to an average radiation power density of 4 kW/cm^2; the peak power in a 100 ps pulse was almost 8 MW/cm^2. Experimental estimates of the diffraction efficiency of the elements coated with the antireflection coating [4] are in good agreement with theoretical estimates.

Such applications like imaging, material ablation, generation of continuous optical discharge, and even more exotic for the terahertz range application, namely the field ionization of individual atoms, require focusing of THz radiation [3-5], often with an enhanced focal depth [3].

Non-diffractive Bessel beams with angular orbital momentum (vortex beams) with different topological charges were formed by use of binary phase spiral axicons [6]. Binary phase axicon (BPA) with spiral zone structure and with aperture diameter of 100 mm (Fig. 1a,b) has been realized in [7] by technology similar to described in [3-6].

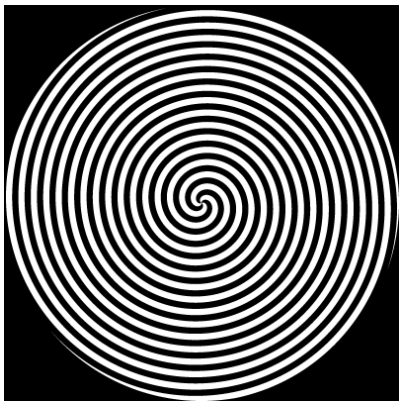

Fig. 1a. Calculated phase of binary diffractive optical element (black, 0; white, π)

Fig. 1b. Photo of realized element

The research has been performed at workstations of the free electron laser NOVOFEL (Budker Institute of Nuclear Physics of SB RAS, Novosibirsk). A high power radiation (in a routine regime, the average power is 50-150 W), a relatively narrow linewidth and the tunability of the radiation enable performing a wide variety of experiments. Vortex beam (Fig. 2) was formed from the NOVOFEL Gaussian beam (wavelength is of 129.5 μm) transformed by binary phase axicon (BPA) with spiral zone structures (Fig. 1) and with aperture diameter of 100 mm.

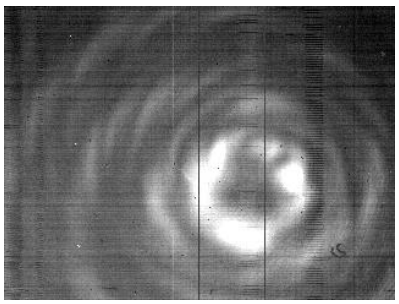

Fig. 2. Intensity distribution measured in the cross-section of beam formed by realized element (Fig. 1)

Vortex beams have great potential for use in free telecommunications and remote sensing [8].
However, lithographic etching has disadvantages in the case of multilevel elements, when an expensive and complicated procedure of alignment of photomask is required [8]. Binary (two-level) elements [3-7], in turn, have limited energy efficiency [8]. The laser ablation technology has been used in [9, 10] for fabrication of multilevel diffractive lens with high energy efficiency. However, diffractive optical elements are designed for working with monochromatic radiation of fixed wavelength [8] only. Fabrication of

terahertz reflective free-form elements for transformation of high-power beams of Free Electron Laser has been considered in [11]. Aluminium elements (spherical and cylindrical mirrors (Fig. 3), reflective axicons) were fabricated by technology of micromilling [11].

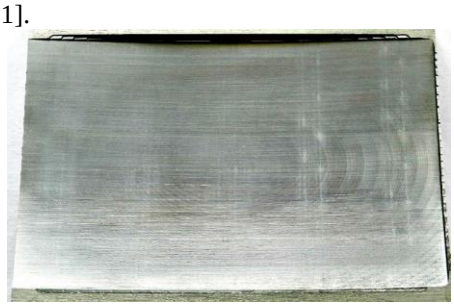

Fig. 3. Fabricated mirror

Realized optical elements were tested in the beam of NOVOFEL at the wavelength of 129.5 μm (Fig.4). The measured diffractive efficiency of the spherical mirror (>94%) is in good agreement with both numerical calculations and theoretical predictions.

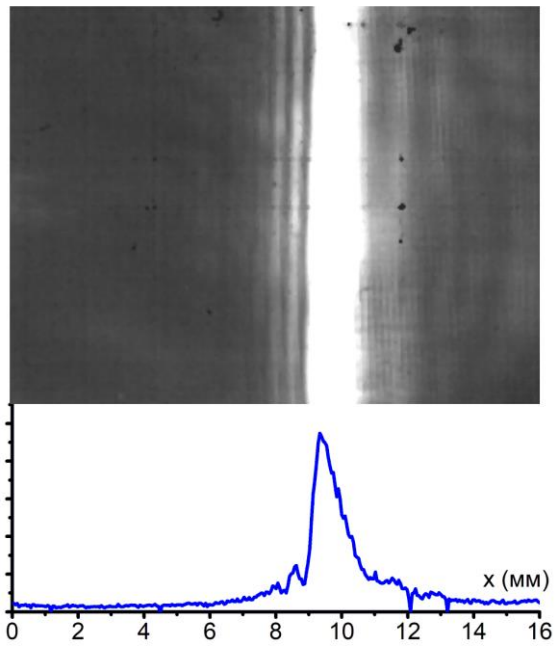

Fig. 4. Intensity distribution in the focal plane of cylindrical mirror

Acknowledgements

The elements were designed under support of the Ministry of Education and Science of the Russian Federation (project 16.7894.2017/6.7). The computer simulation of elements has been realized under support of RFBR grant 16-47-630560.

The terahertz beamline was designed under support of RSF grant 14-50-00080. The work was carried out in the collective research center supported by the Ministry of Education and Science of the Russian Federation, project RFMEFI62117X0012.

References

1. *Knyazev, B.A., Kulipanov, G.N., Vinokurov, N.A.* Novosibirsk terahertz free electron laser: instrumentation development and experimental achievements // Measurement Science and Technology. 2010. V. 21, No. 5. 054017, PP. 1-13

2. *Kulipanov, G.N., Bagryanskaya, E.G., Chesnokov, E.N., Choporova, Yu.Yu., Gerasimov, V.V., Getmanov, Ya.V., Kiselev, S.L., Knyazev, B.A., Kubarev, V.V., Peltek, S.E., Popik, V.M., Salikova, T.V., Scheglov, M.A., Seredniakov, S.S., Shevchenko, O.A., Skrinsky, A.N., Veber, S.L., Vinokurov, N.A.* Novosibirsk Free Electron Laser—Facility Description and Recent Experiments // IEEE Transactions on Terahertz Science and Technology. 2015. V. 5, No. 5, PP. 798-809

3. *Agafonov, A.N., Volodkin, B.O., Kachalov, D.G., Knyazev, B.A., Kropotov, G.I., Tukmakov, K.N., Pavelyev, V.S., Tsypishka, D.I., Choporova, Yu.Yu., Kaveev, A.K.* Focusing of Novosibirsk Free Electron Laser (NovoFEL) radiation into paraxial segment // Journal of Modern Optics. 2016. V. 63, No. 11, PP. 1051-1054.

4. *Agafonov, A.N., Volodkin, B.O., Kaveev, A.K., Knyazev, B.A., Kropotov, G.I., Pavel'ev, V.S., Soifer, V.A., Tukmakov, K.N., Tsygankova, E.V., Choporova, Yu.Yu.* Silicon diffractive optical elements for high-power monochromatic terahertz radiation // Optoelectronics, Instrumentation and Data Processing. 2013. V. 49, No. 2, PP. 189-195.

5. *Agafonov, A.N., Volodkin, B.O., Volotovsky, S.G., Kaveev, A.K., Knyazev, B.A., Kropotov, G.I., Tykmakov, K.N., Pavelyev, V.S., Tsygankova, E.V., Tsypishka, D.I., Choporova, Yu.Yu.* Silicon optics for focusing of terahertz laser radiation in a given two-dimensional domain// Computer Optics. 2013. V. 37, No. 4, PP. 464-470 (In Russ.).

6. *Knyazev, B.A., · Choporova, Yu.Yu., · Mitkov, M.S., · Pavelyev, V.S., · Volodkin, B.O.* Generation of Terahertz Surface Plasmon Polaritons Using Nondiffractive Bessel Beams with Orbital Angular Momentum // Physical Review Letters. 2015. V. 115, N 16, art 163901.

7. *Pavelyev, V.S., Volodkin, B.O., Tukmakov, K.N., Knyazev, B.A., Choporova, Yu.Yu.* Transmissive Diffractive Microoptics for High-Power THz Laser Radiation // AIP Conference Proceedings. 2018. V. 1989, No. 1, art. 020025.

8. *Computer Design of Diffractive Optics*, edited by V.A. Soifer. Cambridge International Science & Woodhead: 2012.

9. *Volodkin, B.O., Knyazev, B.A., Kononenko, V.V., Kononenko, T.V., Konov, V.I., Pavelyev, V.S., Soifer, V.A., Tukmakov, K.N., Choporova, Yu.Yu.* Fabrication of a multilevel THz Fresnel lens by femtosecond laser ablation // Quantum Electronics. 2015. V. 45, No. 10, PP. 933 –936.

10. *Minkevičius, L., Indrišiūnas, S., Šniaukas, R., Voisiat, B., Janonis, V., Tamošiūnas, V., Kašalynas, I., Račiukaitis, G., Valušis, G.* Terahertz multilevel phase Fresnel lenses fabricated by laser patterning of silicon // Optics Letters. 2017. V. 42, No. 10, PP. 1875-1878.

11. *Pavelyev, V., Agafonov, A., Ahmetova, E., Platonov, V., Knyazev, B.*, Reflective free-form optical elements for focusing of high-power THz radiation // Book of abstracts of International Conference "Synchrotron and Free electron laser Radiation: generation and application" (SFR-2018), PP. 41-42.

.

Nonlinear Transfer of Intense Few Cycle Terahertz Pulse Through Opaque Semiconductors

O. V. Chefonov[1], A. V. Ovchinnikov[1], M. B. Agranat[1], V. E. Fortov[1], E. S. Efimenko[2], A. N. Stepanov[2], T.Ozaki[3], X.Chai[3], X.Ropagnol[3], A.A.Ushakov[4] and A.B. Savel'ev[4]

[1]*Joint Institute for High Temperatures of the Russian Academy of Sciences, Moscow, Russia*
[2]*Institute of Applied Physics of the Russian Academy of Sciences , Nizhny Novgorod, Russia*
[3]*INRS-EMT, Advanced Laser Light Source, INRS, Varennes, Canada*
[4]*Lomonosov Moscow State University, Moscow, Russia*

An ultra-strong terahertz (THz) electric field has become available for experiments recently and this opened feasibility of nonlinear terahertz optics. Record-breaking results have been obtained using synchrotron radiation sources (pulse energy W_{THz} > 100μJ, electric field strength E_{THz} up to 20 MV/cm in the frequency range > 10 THz) or using optical rectification in nonlinear organic crystals (W_{THz} ~900 μJ, E_{THz} ~50 MV/cm in the frequency range ~ 1 THz).

Self-induced transparency of a medium under the action of terahertz radiation (or bleaching) was previously observed in semiconductors irradiated with a THz field of relatively low strength and increase in transmission was of a few percent only.

We studied the interaction of an intense THz pulse with the n-doped Si sample under the conditions inaccessible to quasi-stationary electric fields. In this work we observed that transmission by energy of the 700 fs THz pulse through n-doped Si sample amounts to as high as ~ 8% with field strength up to 5–7 MV/cm and then gradually decreases nearly twofold at higher electric fields of 10–20 MV/cm [1,2]. Analysis of the transmitted pulse waveform demonstrated its strong distortions and generation of higher frequency spectral components at 7–10 MV/cm, and finally a 300-fs single-cycle pulse was observed at a maximum field. Simulations showed that with E_{THz} ~5–7 MV/cm saturation of the electron-phonon collision rate occurs, and THz transmission saturates. Generation of a single-cycle pulse at even higher fields was associated with formation of a thin ionized layer at the front sample's surface during the first intense oscillation of the THz field cutting out subsequent field oscillations and decreasing total transmission.

We used the open-aperture Z-scan technique, based on gradual varying of the THz radiation intensity on the surface of the sample moved along the beam line by a stepping motor, to study nonlinear effects. THz radiation was generated by the optical rectification in the nonlinear organic crystal 4-N,N-dimethylamino-4′-N′methyl-stilbazolium 2,4,6-trimethylbenzenesulfonate (DSTMS), pumped by 100-fs femtosecond laser pulses at a central wavelength of 1240 nm delivered by a Cr:forsterite laser system [3,4]. A broadband THz filter (LPF8.8-47, Tydex) with a cutoff wavelength of 34 μm was placed after the crystal. Two off-axis parabolic mirrors were used as a 5:1 telescope to expand the THz beam. Finally, THz pulses with energy of 6.3 μJ were focused with an off-axis parabolic mirror with a 2" diameter and a focal length of 2" onto the sample to a spot with a radius of $w_0 \simeq 200$ μm at $1/e^2$, measured using the knife edge technique. The duration τ_{FWHM} of the THz pulse measured with a first order autocorrelator (a THz Michelson-type interferometer) was 700 fs at full width at half-maximum (FWHM).

The Golay Cell GC-1D (Tydex) was used to measure THz pulse energy transmitted through the sample. The THz electric field in the time domain after the sample was measured using electro-optical (EO) sampling in a nonlinear bilayer 2.1-mm-thick GaP crystal with a 2-mm-thick GaP (100) and a 0.1-mm-thick GaP (110). Fields strengths at the crystal were low enough to ensure linearity of measurements. This scheme was placed instead of the Golay cell.

Maximal THz field strength reached at z=0 was estimated in two ways. First, we employed the well-known time-averaged Poynting vector approach using data on the energy, spot size and duration of the THz pulse. Second, we fulfilled EOS with a 100-μm thick GaP crystal placed at z=0 with femtosecond laser radiation at 1240 nm as a probe. The both measurements gave an estimate of the maximal THz field strength $E_{THz} \approx 21 \pm 1$ MV/cm at $W_{THz} \approx 105$ μJ.

The sample used was a commercially available n-doped silicon wafer of 245 μm thickness with carrier concentration and mobility of 8.7×10^{16} cm^{-3} and 800 cm^2 V^{-1} s^{-1}, respectively, obtained from Hall effect measurements.

Transmittance of the THz radiation was assessed as the ration of the THz pulse energy passed through the sample to the THz pulse energy without the sample (Fig.1). With increasing maximum electric-field strength above 1 MV/cm a complex nonlinear dynamic of transmission of the 245-μm thick n-doped Si with carrier concentration of 9×10^{16} cm^{-3} was observed. An increase of electron-phonon collision rate (due to an increase of "instantaneous" electron energy) results in the bleaching at electric fields below 5 MV/cm. The maximum transmission by energy was found out ~ 8% that is more than two orders of magnitude higher than with a low-intensity THz pulse. Saturation of the transmission is attributed to saturation of the collision rate at electron energies above 1.5 eV.

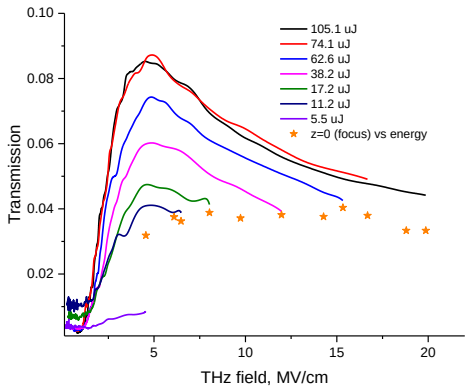

Fig.1. Experimental dependencies of the transmission η on the strength E_{THz} at different pulse energies.

The transmission gradually decreases at higher fields above 7 MV/cm that is related to the onset of ionization by electron impact. Ionization occurs in a thin surface layer during the first intense oscillation of the THz field. This results in efficient reflection and attenuation of subsequent field oscillations leading to formation of a single-cycle THz pulse with sharp rising edge and broad spectrum (Fig.2). This pulse propagates deeper into the sample under the bleaching conditions. The observed effect strongly depends on the spatial energy distribution over the THz beam cross section and, in our experiments, the maximum transmittance was observed out of the focal plane.

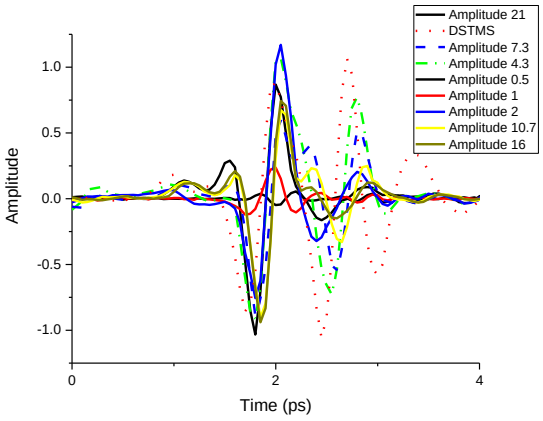

Fig.2. Waveforms of THz pulses without (DSTMS) and with the sample at different THz failed strengths.

To make deeper insight into the spectral-temporal changes of the THz pulse, preliminary numerical simulations of nonlinear propagation of an intense THz pulse through a silicon plate were performed. The Finite Difference Time Domain method was used to solve numerically the 1D Maxwell's equations for the electromagnetic field together with equations for plasma currents and carrier concentration. Dependencies of both the collision and impact ionization rates in Si on the E_{THz} were taken into account when calculating the current.

We also studied the nonlinear carrier dynamics in n-doped semiconductor InGaAs [5]. Intense THz pulses have pushed the nonlinear responses of doped InGaAs semiconductor into a new regime that involves interband carrier dynamics. Intraband heating dominates the overall THz responses and therefore doped semiconductor can still be a good candidate for the applications of saturable absorber.

The work was supported by Russian Science Foundation no. 17-19-01261. Experiments were performed using the unique scientific facility "Terawatt Femtosecond Laser Complex" in the Center "Femtosecond Laser Complex" of the Joint Institute for High Temperatures of the Russian Academy of Sciences.

References

1. *Chefonov O.V., Ovchinnikov A.V., Romashevskiy S.A., Chai X., Ozaki T., Savel'ev A.B., Agranat M.B., Fortov V. E.* Giant self-induced transparency of intense few-cycle terahertz pulses in n-doped silicon // Optics Lett. 2017. V.42, No 23. P.4889–4892.
2. *Chefonov O.V., Ovchinnikov A.V., Agranat M.B., Fortov V.E., Efimenko E.S., Stepanov A.N., Savel'ev A.B.* Nonlinear Transfer of Intense Few Cycle Terahertz Pulse Through Opaque n-doped Si // submitted to Phys.Rev.B.
3. *Vicario C., Ovchinnikov A. V., Ashitkov S. I., Agranat M. B., Fortov V. E., Hauri C. P.* Generation of 0.9-mJ THz pulses in DSTMS pumped by a Cr:Mg_2SiO_4 laser // Opt. Lett. 2014. V.39, No.23. P. 6632-6635.
4. *Vicario C., Jazbinsek M., Ovchinnikov A. V., Chefonov O. V., Ashitkov S. I., Agranat M. B., Hauri C. P.* High efficiency THz generation in DSTMS, DAST and OH1 pumped by Cr:forsterite laser // Opt. Express 2015. V.23, No.4. P.4573-4580.
5. *Chai X., Ropagnol X., Ovchinnikov A., Chefonov O., Ushakov A., Garcia-Rosas C. M., Isgandarov E., Agranat M., Ozaki T., Savel'ev A.* Observation of crossover from intraband to interband nonlinear terahertz optics // submitted to Optics Letters.

Relaxation of Coulomb States in Semiconductors Probed by FEL Radiation

R.Kh. Zhukavin[1], K.A. Kovalevsky[1], V.V. Tsyplenkov[1], S.G. Pavlov[2], H-W. Hübers[2,3], Yu.Yu. Choporova[4,5], B.A. Knyazev[4,5], J.M. Klopf[6], B. Redlich[7], N.V. Abrosimov[8], Yu.A. Astrov[9], V.N. Shastin[1]

[1]Institute for Physics of Microstructures, Nizhny Novgorod, Russia, zhur@ipmras.ru
[2]Institute of Optical Sensor Systems, German Aerospace Center (DLR), Berlin, Germany
[3]Department of Physics, Humboldt-Universität zu Berlin, Berlin, Germany
[4]Budker Institute of Nuclear Physics, Novosibirsk, Russia
[5]National Research Novosibirsk State University, Novosibirsk, Russia
[6]Helmholtz-Zentrum Dresden-Rossendorf, Dresden, Germany
[7]FELIX Laboratory, Radboud University, Institute of Molecules and Materials, Nijmegen, The Netherlands
[8]Leibniz-Institut für Kristallzüchtung (IKZ), Berlin, Germany
[9]Ioffe Institute, St. Petersburg, Russia

The typical semiconductors such as silicon and germanium with embedded donors and acceptors have been intensively studied since 1950th [1]. The main reason was the importance of doped semiconductors in the production of various electronic devices based on the properties of p-n junction or Schottky-junction. The new interest to Coulomb centers in semiconductors has arisen from several new directions including single-atom electronics, quantum logic and lasing based on impurity centers. For use of Coulomb centers in the frame of any of those fields one should know such properties of bound electron as energy spectrum and relaxation rates. The experimental methods being used for the investigations compose a very broad set of different techniques involving transport and optics and their combinations under various conditions. Last two decades the appearance of new user facilities based on THz free electron lasers (FELs) emitting high power short THz pulses provides the unique opportunity for studying of impurity centers in semiconductors under resonant excitation of chosen energy levels using single color pump-probe technique [2-4]. In particular, the lifetimes of different donors and acceptors in silicon have been measured to localize the time scale of the existing relaxation rates. More recently similar experiments have been performed to explore impurities in germanium. Here the authors present a review of pump-probe experiments devoted to lifetime measurements of excited donor states in silicon and germanium under the uniaxial stress.

As well known the relaxation of shallow donor electrons in semiconductors under low temperatures is governed by the emission of acoustic or optical phonons. The elemental semiconductors such as silicon and germanium have multi-valley structure of the conduction band that, together with appropriate energy gaps between states of the Coulomb centers, allow intervalley electron scattering processes. In silicon those are accompanied by the emission of f-type or g-type optical or acoustic phonons. The former corresponds to e.g. [100]-[010] transition while the latter to [100] – [-100] transition in the reciprocal space. The uniaxial stress applied along [100] crystal axis removes the degeneracy resulting in splitting of valleys and corresponding energy levels. Thus uniaxial stress can modify relaxation rates if changes the energy gaps. Fig. 1 demonstrates the energy diagram of phosphorus donor in silicon under the stress as an example. The excited states move parallel to their "parent" valleys while the singlet ground state $1s(A_1)$, which contains equal contributions from 6 valley under zero stress, moves nonlinearly losing the contribution of upper valleys.

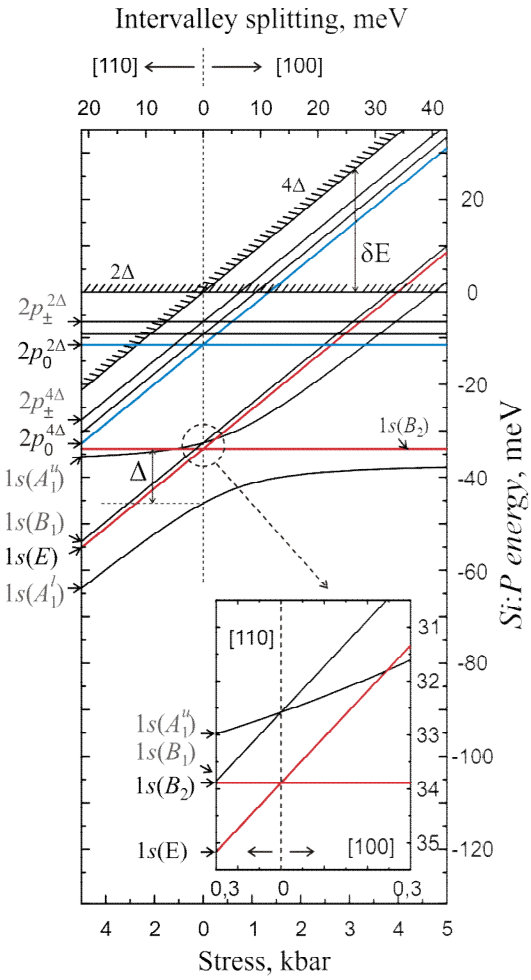

Fig. 1. Energy diagram for phosphorus donor in silicon as a function of uniaxial stress along [110] (left) or [100] (right) crystallographic orientation. Only lower excited states and ground states are shown as well as position of conduction band valleys 2Δ and 4Δ.

The silicon and germanium crystals doped by different donors were taken for sample preparation. The silicon samples were cut along 100 axis while germanium samples were cut along 111 axis. Those directions were chosen to provide the maximum valley splitting for given stress value. Typical donor concentrations were in the range of N_D=1-5×10^{15} cm^{-3}. The samples were shaped into parallelepipeds with dimensions of ~7×5×2 mm^3. Each sample was placed into the special module designed to apply uniaxial stress. The stress module containing one sample and individual stress value was mounted in an optical liquid helium flow cryostat and cooled to about 5 K. The achieved stress value in each module was estimated from the splitting of the donor levels as measured by absorption spectroscopy. Relaxation times of particular electronic states were derived from the time-resolved pump-probe technique. This involved the frequency-selective excitation of the investigated sample with an optical pulse, where the excitation photon energy corresponded to the energy of the transition between the probed electronic states. To measure the characteristic decay time τ, the pulse duration of optical excitation must be much shorter than τ and the time delay between pump and probe pulses must be appropriate to resolve τ. The overall data set was obtained using pump-probe experimental setups at several free electron laser facilities: FELIX (The Netherlands), FELBE (Germany) and NovoFEL (Russia). Details of the pump-probe setups are given elsewhere. Spectral width of the FEL emission on half width on half maximum (FWHM) was better than 1 % of a FEL wavelength. The typical micropulse duration was about 10 ps for FELIX and FELBE and 100 ps for NovoFEL.

Fig. 2 demonstrates the pump-probe signals obtained for Si:P stressed along [100] when pumped into the lower stress component of $2p_0$ level for two values of uniaxial stress – 80 and 650 bar. It is clear seen from the picture that higher stress value results in longer lifetime indicating suppression of the f-type phonon emission. Similar results have been obtained for other donor in silicon such as bismuth and arsenic. It has been obtained that typical lifetimes for donors in germanium are much longer (0.5-3 ns) than for acceptors in germanium (150-250 ps) as well as donors (100-200 ps) and acceptors (30-100 ps) in silicon. The stress applied along [111] axis for Ge:Sb results in increase of lifetime for $2p_{\pm}$ level from 1.8 ns to about 3.2 ns that can be explained by switching off the intervalley relaxation.

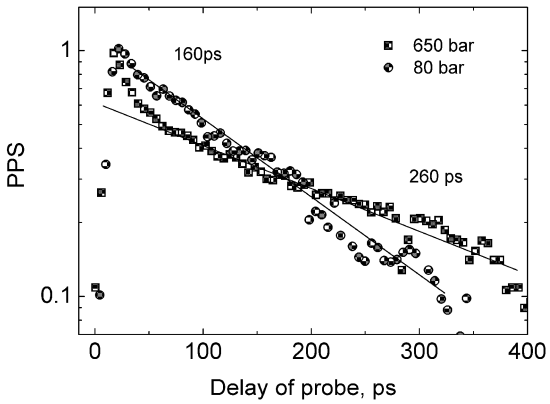

Fig. 2. Pump-probe signal for Si:P under two values of uniaxial stress (80 bar and 650 bar) along [100].

This work was partly supported by the joint German-Russian project of the Russian Foundation for Basic Research (RFBF Project No. 18-42-520064, 18-502-12077-DFG) and of the Deutsche Forschungsgemeinschaft (DFG No. 389056032).

References

1. *Ramdas, A. K., Rodriguez, S.* Spectroscopy of the solid-state analogues of the hydrogen atom: donors and acceptors in semiconductors, Rep. Prog. Phys. 1981, V. 4, P. 1291-1387.

2. *Hübers, H.-W., Pavlov, S. G., Lynch, S. A., Greenland, Th., Litvinenko, K. L., Murdin, B., Redlich, B., van der Meer, A. F. G., Riemann, H., Abrosimov, N. V., Becker, P., Pohl, H.-J., Zhukavin, R. Kh., Shastin, V. N.* Isotope effect on the lifetime of the $2p_0$ state in phosphorus-doped silicon // Phys. Rev. B. 2013. V. 88, P. 035201(1-5).

3. *Pavlov, S. G., Deßmann, N., Pohl, A., Shuman, V. B., Portsel, L. M., Lodygin, A. N., Astrov, Yu. A., Winnerl, S., Schneider, H., Stavrias N., van der Meer, A. F. G., Tsyplenkov V. V., Kovalevsky, K. A., Zhukavin, R. Kh., Shastin, V. N., Abrosimov, N. V., Hübers, H.-W.* Dynamics of nonequilibrium electrons on neutral center states of interstitial magnesium donors in silicon // Physical Review B. 2016. V. 94, P. 075208(1-8).

4. *Choporova, Yu. Yu., Gerasimov, V. V., Knyazev, B. A., Sergeev, S. M., Shevchenko, O. A., Zhukavin, R. Kh., Abrosimov, N. V., Kovalevsky, K. A., Ovchar, V. K., Hübers, H-W., Kulipanov, G. N., Shastin, V. N., Schneider, H., Vinokurov, N. A., Kulipanov, G. N.* First terahertz-range experiments on pump–probe setup at Novosibirsk free electron laser // 2016. Physics Procedia. V. 84, P. 152-156.